Rigidity percolation in dispersions with a structured viscoelastic matrix

M. W. L. Wilbrink and M. A. J. Michels
Technische Universiteit Eindhoven, Group Polymer Physics, Department of Applied Physics, P.O. Box 513, 5600 MB Eindhoven, The Netherlands

W. P. Vellinga and H. E. H. Meijer
Technische Universiteit Eindhoven, Materials Technology, Department of Mechanical Engineering, P.O. Box 513, 5600 MB Eindhoven, The Netherlands

(Received 17 May 2004; published 22 March 2005)

This paper deals with rigidity percolation in composite materials consisting of a dispersion of mineral particles in a microstructured viscoelastic matrix. The viscoelastic matrix in this specific case is a hydrocarbon refinery residue. In a set of model random composites the mean interparticle surface-to-surface distance was controlled, changing particle volume fraction φ and particle number density independently. This was achieved by mixing two sets of monodisperse particles with widely differing radii (0.35 μm and 17.5 μm) with the matrix. A scaling exponent of 3.9 ± 0.6 for the storage modulus G' vs φ-φ_c was observed above a threshold φ_c, in good agreement with theoretical values for rigidity percolation. It is found that at the rigidity-percolation threshold the pore structure, as characterized by the mean surface-to-surface distance for the filler, rather than the filler volume fraction, is similar for different types of composites. This behavior is explained from the internal structure of the viscoelastic matrix, which consists of fractal solid aggregates dissolved in a viscous medium; the effective radius of these aggregates and the mean surface-to-surface distance together determine whether or not the aggregates are capable of providing rigidity to the composite. The explanation is further supported by a qualitative comparison with effective-medium calculations. These indicate that the observed breakdown of time-temperature superposition near φ_c is due to the appearance of a time scale characteristic for the mechanical interplay between the viscous binder phase and the purely elastic solid particles.

DOI: 10.1103/PhysRevE.71.031402 PACS number(s): 61.43.Hv, 83.80.Hj, 82.70.Gg

I. INTRODUCTION

This paper deals with the mechanical properties of model random composites consisting of a viscoelastic matrix with dispersed hard mineral particles. More specifically, the viscoelastic matrix in the composites treated here is a hydrocarbon residue from a crude-oil refinery process. A crude oil is a complex colloidal system, of which in the refinery 60%–70% can be easily processed by normal and vacuum distillation and thermal or catalytic cracking. The residual hydrocarbon material from such processes is called a residue. A main commercial use is as a "binder" for mineral particles ("fillers") to form asphalt mixes for paving applications. Such residues are mixtures of a broad range of hydrocarbon chemical species differing by their molar masses, aromatic and aliphatic structures, and polarity. Usually a separation is made into four pseudocomponents: saturates, aromatics, resins, and asphaltenes (so-called SARA fractions). Asphaltenes are defined as that part of the residue that is insoluble in paraffinic solvents (e.g., *n*-heptane) but soluble in toluene. The remaining heptane-soluble mixture of saturates, aromatics and resin molecules is called the "maltene phase"; the toluene-insoluble part is the "coke."

From the literature [1–3] the following picture of the asphaltene fraction arises. The asphaltenes are heterocyclic aromatic sheets with molecular masses $M_W > 1000$ a.u., with attached alkyl side chains restricted to the plane of the sheet. The side chains may contain, in addition to hydrogen and carbon, heteroatoms such as O, N, and S. The aromatic sheets typically have a diameter of 1.2–2.0 nm and are capable of associating perpendicular to the plane of the sheet in the presence of nonpolar or slightly polar solvents to form irregular π stacks a few nanometers in height [4]. These asphaltene stacks, which are insoluble in the maltene phase, are believed to be peptised by a solvation shell of resin molecules to form primary aggregates that are often called "micelles"; whether they are true micelles in a thermodynamic sense is still a matter of debate. Depending on the degree of aromaticity of the maltene phase and the chemical nature and volume fraction of the asphaltenes, the micelles may either move freely through the maltene phase or form larger aggregates. Results of past small angle x-ray scattering and wide angle x-ray scattering (SAXS/WAXS) experiments on several residues from cracking processes were consistent with the presence of large ($R > 200$ nm) fractal aggregates of asphaltene stacks, with aggregate radius increasing with increasing asphaltene thermodynamic instability; the fractal dimension of these aggregates was invariably $D_f = 1.7–1.8$, indicating diffusion-limited growth as their origin [5,6].

Summing up, a crude-oil residue can be viewed as a colloidal dispersion of stacked asphaltenes in resin shells, dispersed in a maltene matrix. The volume fraction of asphaltenes, their chemical structure, the resulting colloidal state, and the level of asphaltene aggregation can vary strongly between different residues, and this asphaltene behavior is thought to be the key factor determining the binder viscoelasticity. Furthermore, upon mixing of the binder with mineral aggregates, composites made from different residues may show widely differing mechanical behaviour: some may flow rather easily; others may upon appropriate processing

show considerable flexural strength. Recently strengths up to 9 MPa in three-point bending have been reported, similar to that of concrete [7]. The origin of this disparity in mechanical properties has again been looked for in the state of the asphaltene fraction, but as of yet a clear physical understanding of their role in the composites is lacking. To contribute to such a physical understanding was the main aim of the work presented here, and the focus was on identifying possible mechanical percolation behavior.

Experimental evidence for rigidity (or elasticity) percolation in dispersions of an elastic filler in a viscous medium can be found at various places in the literature. In such cases it is found that the storage (elastic) modulus G' and filler volume fraction φ are related according to the following scaling law:

$$G' \propto (\phi - \phi_c)^{\alpha}, \tag{1}$$

with φ_c the percolation threshold. A number of these results will be discussed in some more detail in Sec. IV, here we will only mention a particularly relevant example recently shown by Trappe and Weitz [8]. They studied the mechanical behavior of suspensions of solid carbon-black in purely viscous base stock oil and observed the critical onset of an elastic network on increasing the volume fraction φ of carbon-black particles or their attractive interaction U above certain critical values φ_c and U_c, respectively. They also noted that $\varphi_c = \varphi_c(U)$ and $U_c = U_c(\varphi)$, as had been previously found in other systems [9]. It may therefore be expected that a similar phenomenon occurs in a dispersion such as considered here, of hard mineral-filler particles in a structured viscoelastic matrix (the maltene phase with the asphaltene aggregates). It merely adds an extra filler (the hard mineral) in a situation analogous to that described above (the elastic asphaltene aggregates in the viscous maltene phase). So the hypothesis under investigation in this paper is that the fractal asphaltene aggregates in the binder and the mineral particles may *together* create a percolating network of particles providing rigidity to the composite.

Clearly, characteristic length scales of the fractal aggregates as well as of the "pore" space in between the mineral particles are of crucial importance. Only if a characteristic interparticle distance is of the same order as the characteristic size of the asphaltene aggregates can a percolating network be expected to arise in the first place. Therefore we hypothesize that the critical volume fraction reflects an internal length scale and is to be related to the particle size distribution function.

In this paper we present the results of a systematic experimental approach to investigate the two hypotheses mentioned above, in which this possible interplay between mineral-filler particles and asphaltene aggregates in the binder was investigated. The key idea has been to produce qualitatively different mechanical behavior in a set of model composites in which a length scale characteristic for the distance between filler particles is varied, using different volume fractions of filler and different filler sizes independently. Details of the experimental procedures are described in Sec. II. Our experimental results are presented in Sec. III. In the subsequent discussion (Sec. IV) it is shown that the experimental results support our hypothesis and are in agreement with theoretical predictions in the literature on rigidity percolation. In Sec. IV, first, the observed scaling properties of the moduli as a function of particle volume fraction and dispersion are discussed. Literature results on elasticity percolation are discussed here. Second, the dependence of the percolation threshold on the relevant length scales in the experiments is discussed. Since determination of characteristic lengthscales in bidisperse or polydisperse random sphere packings is a rather specialistic problem, relevant results that are available in the literature will only be briefly introduced and shown in some more detail in Appendixes A and B. Third, the breakdown of time-temperature superposition is adressed by making a comparison with effective-medium calculations. Conclusions follow in Sec. V.

II. EXPERIMENTAL APPROACH

A. Model composites

A specific type of refinery residue, known to show very desirable properties in commercial composites, is used as a binder in this study. This residue has a density of 1.094 g/cm^3 and contains 24.9 wt% of asphaltenes; this amounts to approximately 19 vol% of asphaltenes. Two kinds of filler were used. The first are monodisperse glass beads (GB's) with a radius $R_{GB}=17.5$ μm and a density of 2.46 g/cm^3 (Whitehouse Scientific Ltd., Chester, UK). The second type of filler consists of monodisperse, calcium-stearate-coated, $CaCO_3$ "Super-Pflex" particles (SP's), with a radius $R_{SP}=0.35$ μm and a density of 2.7 g/cm^3 (Specialty Minerals Inc., Bethlehem, PA, USA). The shear modulus G_{SP} of the SP particles is assumed to be equal to the shear modulus of $CaCO_3$, 35 GPa. The calcium-stearate coating on the SP particles is designed to avoid clustering.

Composites were produced as follows. A balance with a sensitivity of 0.1 mg was used to weigh filler and binder; the volume fraction of filler was calculated from the density of binder and filler. Preparation of the composites has been standardized for all samples. A cup with binder is heated to 210 °C on a simple heating plate and subsequently held at this temperature, upon which the binder is melted for 15 min. Then, for 5 min, the filler is slowly added under constant mixing by hand. After all the filler has been added, an additional 10 min of mixing by hand follows. Subsequently the dispersion is poured into coin-shaped moulds (with diameters of 8 mm and 20 mm) in which it cools down to room temperature. Finally, the samples are stored in sealed plastic bags. Table I gives details of the model composites produced in this way.

B. Rheological measurements

Standard oscillatory-shear experiments were carried out on a strain-controlled rheometer [10]. A 25-mm-diam parallel-plate geometry with a gap of approximately 1.5 mm was used at the higher temperatures. At lower temperatures, an 8-mm-diam geometry was used with a gap of approximately 2.5 mm. Experiments were performed at temperatures ranging from −10 °C to 240 °C. Frequency sweeps

TABLE I. Properties of all composites referred to in the text: volume percentage of SP (radius 3.5 μm) and GB (radius 17.5 μm) fillers, mean surface-to-surface distance $\lambda_P(0)$ for a test particle with zero radius, and temperature ranges in oscillatory-shear experiments.

	SP vol%	GB vol%	$\lambda_P(0)/R_{SP}$	T range (°C)
	0	0	-	10–120
	50	0	0.18	30–200
	30	0	0.36	30–200
	20	0	0.54	20–160
	15	0	0.69	10–160
SP	13	0	0.77	10–160
	10	0	0.92	10–150
	10	10	0.85	30–160
	8	12	0.97	40–160
SP-GB	6	14	1.15	30–160
	5	15	1.27	30–160
	0	20	27.0	30–140
	0	30	18.1	30–140
GB	0	50	9.0	40–130

from 0.4 rad/s to 100 rad/s were carried out every 10 °C, starting at low T. The absolute shear modulus $G^*(\omega) = |G(\omega)|$ and phase angle $\delta(\omega) = \arctan [G''(\omega)/G'(\omega)]$ were measured as a function of the angular frequency ω. Prior to each frequency sweep a strain sweep was performed at 5 rad/s to estimate the strain interval of linear response. Measurements were then performed at the maximum strain for which the nonlinearity in G^* was less than 2%. Table I shows the temperature ranges for all experiments. Master curves were created [11] by shifting each set of frequency-sweep data along the ω axis to a reference temperature of 40 °C. The curves were shifted using a least-squares-minimization algorithm which optimises the overlap between adjacent data sets. In the following, whenever reference is made to master curves, G^*, G', G'', and δ are short for the quantities $G^*(a_T\omega)$, $G'(a_T\omega)$, $G''(a_T\omega)$, and $\delta(a_T\omega)$, respectively, with a_T a temperature-dependent shift factor and $a_T\omega$ a scaled frequency (see Sec. III). Use of master curves implies invoking the time-temperature superposition (TTS) principle. However, it will become clear that the TTS principle is not applicable to all composites investigated in this paper. As an alternative method to represent the data, so-called Black diagrams [12] are used, in which $\delta(\omega)$ is plotted as a function of $G^*(\omega)$. In a Black diagram raw data are plotted, so TTS is not invoked. Roughly speaking, if all data sets together form a smooth curve in a Black diagram, TTS holds.

III. RESULTS

A. Binder

Figure 1 shows the master curves (T_{ref}=40 °C) of G^* and δ as a function of scaled frequency $a_T\omega$ for the unmodified binder. The shift factors a_T for the binder master curve very well obey the Williams-Landel-Ferry (WLF) equation [11]

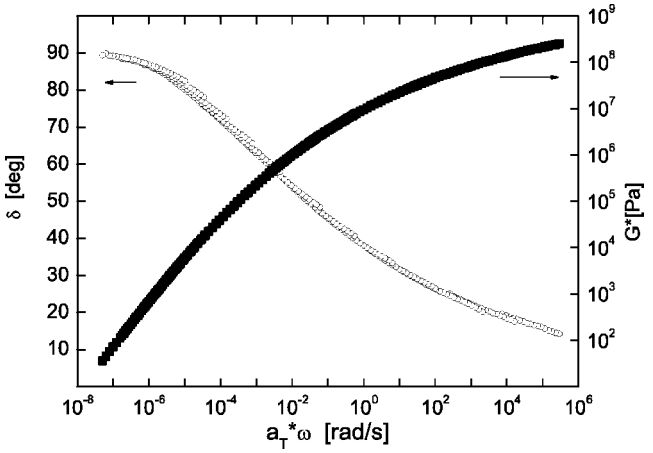

FIG. 1. Viscoelastic behavior of pure binder: absolute modulus G^* and phase angle δ vs scaled frequency $a_T\omega$.

$$^{10}\log(a_T) = -\frac{c_1(T - T_{ref})}{c_2 + (T - T_{ref})}, \tag{2}$$

with c_1 and c_2 equal to 23 K and 195 K, respectively. In the limit $\omega \to \infty$, G^* approaches 1 GPa. This value is consistent with that reported by van der Poel [13] as the asymptotic limit of the shear stiffness of all bitumens at low temperatures (equivalent to high scaled frequencies). At high temperatures or low scaled frequencies, the binder behaves in a fully viscous way [$\delta(\omega)$=90°], so G'' dominates G^*. The slope of the master curve equals 1 in this region, as expected.

B. Model composites

Figures 2(a) and 2(b) show G^* and δ vs scaled frequency $a_T\omega$ for the SP composites, (with $0 \leqslant \varphi_{SP} \leqslant 0.5$; see Table I). It is immediately obvious that the viscoelastic properties of the composite materials strongly depend on φ_{SP}. Several points deserve attention.

G^* is more or less constant at low scaled frequencies for materials with $\varphi_{SP} \geqslant 10\%$. But the value of these plateaus in G^* is seen to depend sensitively on φ_{SP}. Furthermore, at the onset of the plateau's in G^*, δ reaches a maximum, indicating that on further decreasing ω the material gets more elastic. However, at still lower $a_T\omega$, δ increases again with decreasing ω. The maximum of δ is observed to decrease for increasing φ_{SP}.

The Black diagram of these results, Fig. 2(c), shows perhaps more clearly that coincidence of the plateau onset in G^* and the decrease in δ is rather sudden on changing the filler content. The behaviour of the materials with $\varphi_{SP}=0$ and $\varphi_{SP}=0.1$ is quite similar, whereas the behavior of the materials with $\varphi_{SP} \geqslant 0.13$ strongly deviates from these two. The qualitative change in behavior occurs somewhere around $\varphi_{SP}=0.1$, as was already clear from Fig. 2(a). Moreover, Fig. 2(b) indicates that TTS does not hold for the samples with high φ_{SP}, as each separate data set is clearly distinguishable, especially in the case of the sample with $\varphi_{SP}=0.5$.

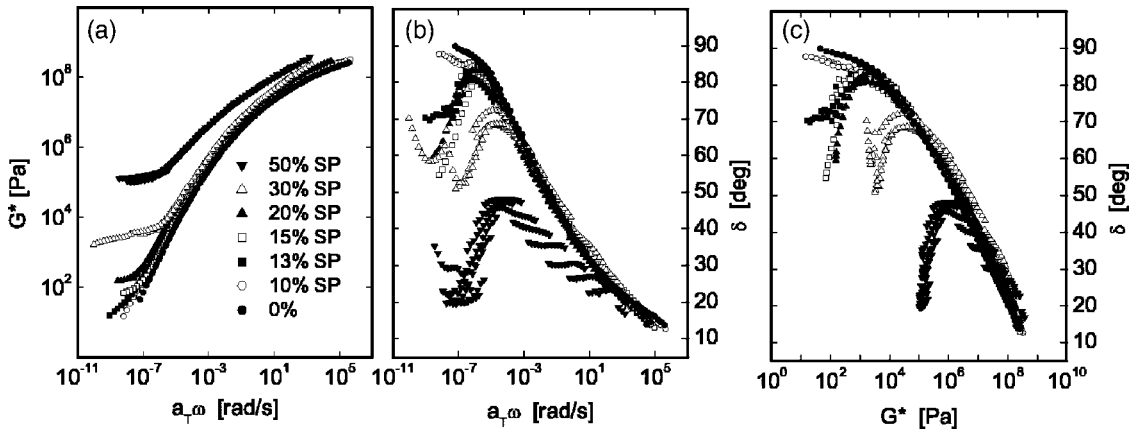

FIG. 2. Viscoelastic behavior of SP composites, with $\varphi_{tot}=\varphi_{SP}$. (a) G^* and (b) δ vs scaled frequency $a_T\omega$. (c) Black diagram of δ vs G^*.

In the SP composites the level of the plateau in G^* depends sensitively on φ, as was shown in Fig. 2(a). The plateau in combination with the decrease in δ indicates a sharp increase of the storage modulus G'. In Fig. 3(a) plateau values of G' and of the loss modulus G'' at 160 °C and 1 rad/s (G'_{pl} and G''_{pl}) are plotted against φ. Sharp increases of G' and G'' above $\varphi \approx 0.1$ are obvious, although the increase in the value of G'' is less pronounced than that in G'. Since it is assumed that this behavior originates from the percolation of an elastic network in the mixture, it may be postulated that G' will behave according to a scaling law typical for percolation, as given in Eq. (1). The scaling exponent α and the percolation threshold φ_c were determined from a nonlinear least-squares fit to the data: $\alpha=3.9\pm0.6$ and $\varphi_c=0.093\pm0.005$. Figure 3(b) shows $^{10}\log G'$ vs $^{10}\log(\varphi\text{-}\varphi_c)$ for this best fit.

Of interest now is the question whether rigidity percolation can also be observed in a series of composites in which φ_{tot} is kept constant and the geometry of the pore volume or the mean surface-to-surface distance $\lambda_p(R)$ is changed. To investigate this, SP-GB composites were used with a mix of SP and GB as filler. In all samples $\varphi_{tot}=\varphi_{SP}+\varphi_{GB}=0.2$. Figure 4(a) shows G^* and δ versus scaled frequency for the SP-GB composites, and Fig. 4(b) shows the corresponding Black diagram. Similar phenomena can be observed as for the SP composites shown in Figs. 2(a) and 2(b), although less pronounced because of the lower maximum filler content. Plateau's are observed for SP-GB composites with $\varphi_{SP} \geqslant 8\%$ and $\varphi_{SP}+\varphi_{GB}=0.2$.

IV. DISCUSSION

The points discussed in this section are the percolation behavior (scaling behavior as well as the percolation threshold), the breakdown of time-temperature superposition, and the relation between these points.

A. Rigidity percolation

1. Scaling behavior

In Sec. III the appearance of plateau's in G^* at low scaled frequency was shown, both for SP composites and SP-GB composites. From the exponent of the scaling law, evidence was given that this behaviour is caused by the formation of a percolating elastic network.

As is clear from the Introduction the critical onset of an elastic network, best known as elasticity or rigidity percolation, is anticipated in the composites. It is generally accepted that the real part G' of the shear modulus will near the percolation threshold scale according to Eq. (1). In numerical simulations of percolating elastic networks, bonds may represent central forces as well as bending forces. Whenever bond-bending forces are present the rigidity threshold φ_c is equal to the connectivity threshold. Numerical estimates for the scaling exponent in bond-bending rigidity percolation yield $\alpha \cong 3.75$ in 3D [14]. This value is in accordance with a conjecture by Roux [15] and Sahimi [16] that

$$\alpha = t + 2\nu, \tag{3}$$

where t and ν are the critical exponents for the conductivity and for the correlation length of percolation networks, with

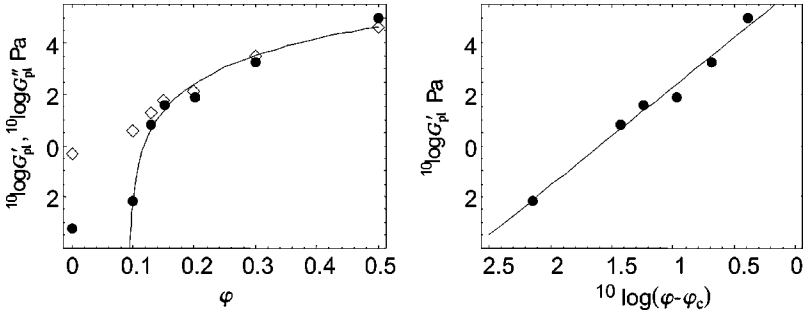

FIG. 3. Rigidity percolation in SP composites. (a) Plateau values G'_{pl} and G''_{pl} (160 °C, 1 rad/s) as a function of φ_{SP} (values for G' at $\varphi_{SP}=0$ and $\varphi_{SP}=0.1$ from extrapolation); the solid line is the best fit of Eq. (1) to the data, with $\alpha=3.86$ and $\varphi_c=0.093$; the data point for G' at $\varphi_{SP}=0$ was excluded from the fit. (b) Log-log plot of G' data and fit from Fig. 5(a), showing rigidity-percolation scaling.

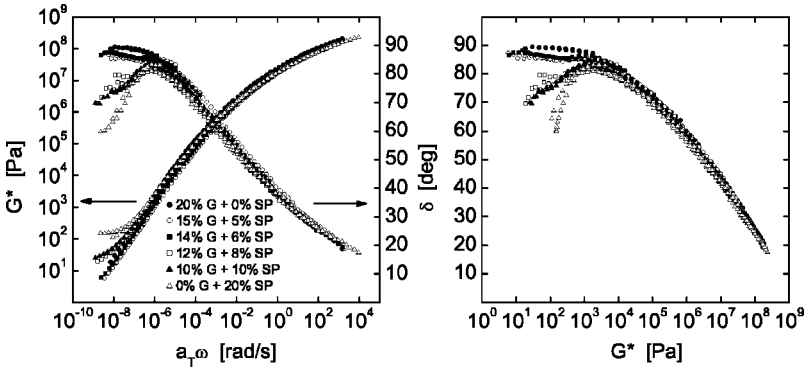

FIG. 4. Viscoelastic behavior of mixed SP-GB composites. (a) G^* and δ vs scaled frequency $a_T\omega$. (b) Corresponding Black diagram.

values of $t=2.0$ and $\nu=0.88$ in three dimensions (3D), respectively. The main simplification made to arrive at this conjecture is in neglecting, in a "nodes-links-blobs" picture of the percolation network, the effect of the "blobs" on the rigidity. The situation for central-force networks is not as clear. It has been proposed, based on numerical simulations, that central-force networks are actually in the same universality class as bond-bending networks, which was subsequently explained with a space-renormalization argument [17]. However, the precision of these results has more recently been called into question [18]. It is concluded that the experimental value $\alpha=3.9\pm0.6$ is in good agreement with the theoretical value of 3.75 for (bond-bending) rigidity percolation as reported in the literature, supporting the hypothesis that rigidity percolation occurs in these materials.

The following qualitative explanation of the formation of the elastic network is proposed: at high temperatures, the viscosity of the maltene matrix is such that the asphaltene particles can move relatively freely through the maltene phase, as a result of their Brownian motion, and aggregation of the asphaltene particles may take place on a relatively short time scale. If these asphaltene aggregates can connect adjacent filler particles, an elastic aggregate may eventually form that consists of *both* filler particles *and* asphaltene aggregates.

2. Relation between microstructure and percolation threshold

In Sec. III the appearance of plateau's in G^* at low scaled frequency was shown, both for SP composites and SP-GB composites. Furthermore, the experiments with the SP-GB composites at constant φ conclusively show that the volume fraction of filler φ *alone* cannot account for all observed phenomena. From the exponent of the scaling law, evidence was given that this behavior is caused by the formation of a percolating elastic network, and it was hypothesized that the network consists of a random network of (polydisperse) spheres *and* fractal asphaltene aggregates. This hypothesis also qualitatively explains why the percolation threshold does not only depend on φ_{tot}, but *also* on the geometry of the filler assembly: a minimum requirement for percolation to occur in the sense described above is that the mean surface-to-surface distance is of the same order as, or smaller than, the effective size of the asphaltene aggregates.

In this section we attempt to test this hypothesis in a quantitative way. In order to do so we compare characteristic length scales in the monodisperse SP and bidisperse SP-GB composites. The expectation is that, because the asphaltene structure is the same in the monodisperse and bidisperse composites, the characteristic length scale at which percolation occurs should be the same in both cases, even if the volume fraction of filler at which percolation occurs differs. Also, one would like to get an estimate of this lengthscale, for two reasons: first, so that it can be compared to typical dimensions of asphaltene aggregates that can be found in literature and, second, because it should be consistent with the absence of percolation in the GB composites at the particle volume fractions used in our experiments. Here we first find an estimate of the length scale from the percolation threshold in the monodisperse SP composites. Subsequently we compare length scales characteristics of the pore space in monodisperse and bidisperse random sphere packings in order to compare the characteristic length at percolation.

With regard to the percolation threshold in the monodisperse composites, the physical picture is that of asphaltene aggregates connecting (elastically interacting with) rigid (mineral filler) spheres. A characteristic size for the aggregates $2R_a$ may be defined such that spheres further apart than $2Ra$ do not interact. If two spheres approach closer than $2R_a$, an interaction may occur provided an asphaltene aggregate is present. Furthermore, the rigid spheres can touch, but cannot interpenetrate. Clearly one can view the distance $2R_a$ as an effective distance characterizing some interaction potential between the rigid spheres caused by the presence of the asphaltenes.

Adopting this view we are interested in the percolation threshold of such a dispersion, as a function of the length $2R_a$.

Particularly relevant to the situation at hand are theoretical and numerical results from models for the percolation in random networks of monodisperse interpenetrable spheres, sometimes called "cherry-pit" models; a useful overview of issues relevant to this subject is [14]. In these descriptions the impenetrable hard cores are usually assigned a radius $R_f=\lambda R_{\mathrm{tot}}$ and the penetrable shell (interaction distance) a width $R_a=(1-\lambda)R_{\mathrm{tot}}$. As was explained above, we associate the impenetrable cores in the model description with the mineral-filler particles and the interaction distance with the characteristic asphaltene aggregate dimension.

A reduced number density $\eta=\rho V_D$ is defined, with ρ the number density and V_D the volume of a D-dimensional sphere with radius R_{tot}. The volume fraction of hard cores is now given by $\eta\lambda^D$. All known numerical results on the per-

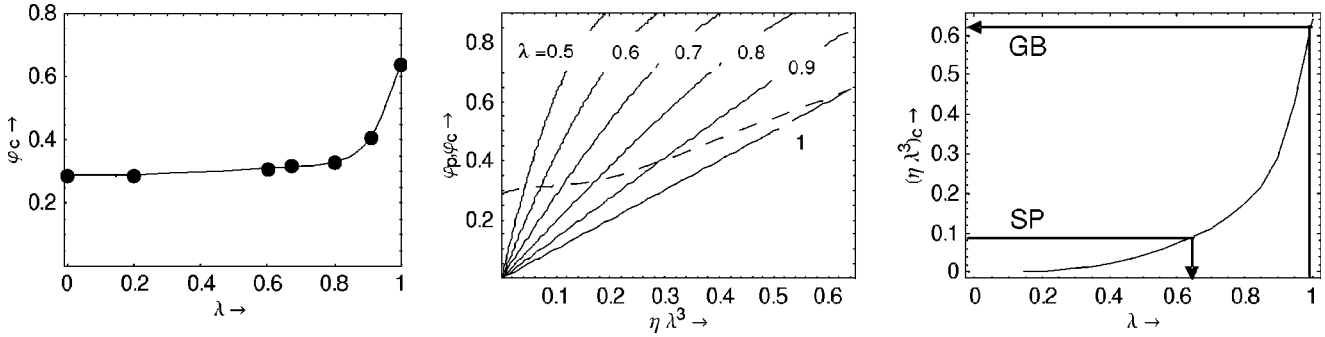

FIG. 5. Connectivity percolation for penetrable spheres. (a) Critical volume fraction φ_c for connectivity percolation vs penetrability parameter λ in a cherry-pit model; points indicate all known values from numerical simulations, the drawn line is a monotonously increasing spline fit through the points [19]. (b) Effective volume fraction φ_p [drawn lines, for indicated values of λ using Eq. (A1)] and critical volume fraction for connectivity percolation φ_c [dashed line; compare Fig. 5(a)] vs hard-core volume fraction $\eta\lambda^3$. (c) Hard-core volume fraction at the connectivity percolation threshold $(\eta\lambda^3)_c$ vs interpenetrability parameter λ.

colation thresholds of such systems in 3D are shown in Fig. 5(a) [14,19], which shows the connectivity percolation threshold φ_c vs λ. Also shown is a monotonously increasing spline fit through the points, which is used below.

The hard-core volume fraction at percolation $(\eta\lambda^3)_c$ can be established with the help of the relations (A1) and (A2) given in Appendix A [14,20].

Figure 5(b) shows $\varphi_p(\eta,\lambda)$ vs $\eta\lambda^3$ for various λ, as well as $\varphi_c(\eta,\lambda)$ vs $\eta\lambda^3$ derived from the spline fit in Fig. 5(a). From the positions of the intercepts of $\varphi_p(\eta,\lambda)$ and $\varphi_c(\eta,\lambda)$, Fig. 5(c) has been derived, showing the hard-core volume fraction at percolation, $(\eta\lambda^3)_c$, vs λ. Figure 5(c) can be directly compared to the experiments with monodisperse assemblies.

For a percolation threshold of 0.093 one finds a value of $\lambda=0.65$ for the penetration parameter; this should correspond to the case of the SP composites, as has been indicated with an arrow in Fig. 5(c). It yields for the asphaltene aggregates a characteristic size of around 190 nm, which is consistent with earlier reports [1,5]. Given this approximate size, the composite of GB filler and asphaltene aggregates would correspond to $\lambda=0.995$ and to a percolation threshold of 0.59 [also indicated in Fig. 5(c)]. This is in accordance with the experimental observation that for $\varphi_{GB}=0.5$ percolation did not occur. We conclude that the interpenetrable sphere description can explain the difference in percolation behavior between the SP and GB composites, if one assumes an effective interaction lengthscale (the asphaltene aggregate size) in the percolation problem.

We are not aware of numerical results on percolation thresholds in cherry-pit models of bidisperse or polydisperse assemblies. This means that an alternative way has to be found to compare the results on the monodisperse composites to results on the bidisperse composites. In general, few experimental or numerical studies seem to exist in which the effect of polydispersity on percolation behavior is systematically studied (see [21], and references therein). However, general results on the geometric properties of such assemblies can be found in [14].

As a characteristic length we use the mean surface-to-surface distance $\lambda_P(R_t)$ that is rigorously defined in [14,22] for general systems of random polydisperse spheres. $\lambda_P(R_t)$ can be calculated for all of the dispersions used in our experiments. It seems useful to briefly repeat the way to calculate $\lambda_P(R_t)$, but since it is not central to the discussion presented here, this is shown in Appendix B.

In the SP-GB composites with $\varphi_{tot}=0.2$ the percolation threshold is around $\varphi_{GB}=0.12$ (and $\varphi_{SP}=0.08$). To relate this result to the percolation threshold $\varphi_c=0.093$ of the monodisperse SP composite, it is argued that if the mean surface-to-surface distance in the monodisperse and bidisperse assemblies is equal, the asphaltene aggregates should cause rigidity percolation in both assemblies. The pore space in monodisperse as well as bidisperse assemblies can be characterized by the mean surface-to-surface distance $\lambda_P(R_t)$, and Fig. 6 shows calculated values of $\lambda_P(R_t)$ for several filler combinations. From Fig. 6 it is clear that the mean surface-to-surface distance in the SP composite with $\varphi_{SP}=0.09$ and the SP-GB composite with $\varphi_{SP}=0.08$ and $\varphi_{GB}=0.12$ are indeed very similar.

Considering the large difference in radius between the SP and GB fillers in these composites, one can arrive at the same

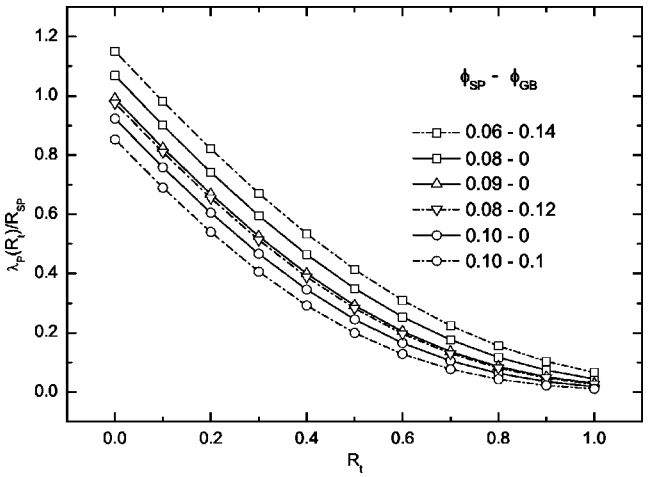

FIG. 6. Mean surface-to-surface distance $\lambda_P(R_t)/R_{SP}$ as a function of test-particle (or asphaltene aggregate) radius R, for a range of experimentally investigated composites.

result in a simpler way. It may be argued that the GB particles are so large and their number density so low that they may simply be represented by an effective volume impenetrable to the SP filler. This increases the effective density of the SP filler to

$$\phi_{\mathrm{SP}}^{\mathrm{eff}} = \frac{\phi_{\mathrm{SP}}}{(1-\phi_{\mathrm{GB}})}. \tag{4}$$

In the case of the percolating SP-GB composite this leads to $\phi_{\mathrm{SP}}^{\mathrm{eff}}=0.091$, which is indeed consistent with the observed rigidity percolation threshold for the SP composites. (The elastic moduli around the percolation threshold are not expected to be the same in both cases, as the moduli and volume fractions of SP and GB filler in the composites are different.)

Both lines of reasoning support the hypothesis that the percolation threshold is determined by the point where characteristic length scales of asphaltene aggregates and mean surface-to-surface distance of the mineral-filler assembly are of the same order.

B. Breakdown of time-temperature superposition

From the experimental data presented in Figs. 1–4, it appears that TTS is applicable for the pure binder as well as for the composites, except for the composites showing rigidity percolation—where TTS fails. In the previous section we have argued that the experimental data are consistent with the formation of a rigid network consisting of both filler particles and asphaltene aggregates. The question addressed in the present section is whether these two phenomena can be related to each other. To investigate this, the experimentally observed behavior of G^* and δ is qualitatively compared to the results of a self-consistent effective-medium theory (EMT).

We define a continuous matrix with complex shear modulus G_1 and volume fraction φ_1 (representing the binder) and inclusions with complex shear modulus G_2 and volume fraction φ_2 (representing the filler). The relationship between G_1 and G_2 and the effective property G_{e} of the medium may be described by the so-called "Bruggeman equation" [23,24]

$$\frac{G_1-G_{\mathrm{e}}}{G_1+\frac{3}{2}G_{\mathrm{e}}}\phi_1 + \frac{G_2-G_{\mathrm{e}}}{G_2+\frac{3}{2}G_{\mathrm{e}}}\phi_2 = 0, \tag{5}$$

which can be restated as

$$G_{\mathrm{e}} = \frac{1}{3}(G_1\psi_1+G_2\psi_2) \pm \frac{1}{3}[(G_1\psi_1+G_2\psi_2)^2+6G_1G_2]^{1/2}, \tag{6}$$

with $\psi_i=\frac{5}{2}\varphi_i-1$ for $i=1,2$. In spite of its symmetrical appearance, this equation can be derived from an initially asymmetric composite model, in which phase 1 is considered a continuous matrix and phase 2 a homogeneous assembly of dispersed filler spheres. This renders the symmetrical Bruggeman form of the effective-medium theory particularly suited to describe the mechanical percolation phenomena at hand. With the reasonable assumption that $G_1^* \ll G_2^*$ one finds

$$G_{\mathrm{e}} \cong \frac{1}{3}(G_1\psi_1+G_2\psi_2) + \mathrm{sgn}(\psi_2)\left\{\tfrac{1}{3}(G_1\psi_1+G_2\psi_2) + \frac{G_1G_2}{(G_1\psi_1+G_2\psi_2)}\right\}, \tag{7}$$

in which the following substitutions are subsequently made:

$$G_i = G_i' + \mathrm{i}G_i'', \tag{8}$$

with $i=1,2,\mathrm{e}$. The further assumption $G_2'' \ll G_1' < G_1'' \ll G_2'$ leads to simple relations showing the main features predicted by Eq. (7) . One finds for the effective storage modulus G_{e}' of the composite material:

$$G_{\mathrm{e}}' \cong \frac{G_1'}{1-\frac{5}{2}\phi_2} \quad (\varphi_2 < 2/5),$$

$$G_{\mathrm{e}}' \cong \frac{G_1'}{\frac{5}{2}\phi_2-1} + \tfrac{2}{3}G_2'\left(\tfrac{5}{2}\phi_2-1\right) \quad (\varphi_2 > 2/5). \tag{9}$$

Equations (10) predict a singularity in G_{e}' around $\varphi=2/5$ and subsequently a large increase above it. The value of this percolation threshold is larger than values observed for the composites in this paper, due to geometric simplifications in our symmetric Bruggeman equation and due to the fact that this EMT does not take finite-ranged interactions between two or more spheres into account. Using the same approximations we get, for G_{e}'',

$$G_{\mathrm{e}}'' \cong \frac{G_1''}{\left|1-\frac{5}{2}\phi_2\right|} \quad (\varphi_2 < 2/5 \text{ and } \varphi_2 > 2/5). \tag{10}$$

So G_{e}'' has a peak around $\varphi_2=2/5$, which will also show in the effective phase angle δ_{e}. G_{e} at the percolation threshold is obtained by substituting $\varphi_2=2/5$ in Eq. (6):

$$G_{\mathrm{e,c}} = \sqrt{\tfrac{2}{3}G_1G_2} \quad (\varphi_2 = 2/5). \tag{11}$$

Any qualitatively realistic description of the mechanical behavior of the composites has to include the frequency-dependent viscoelasticity of the binder. The simplest possible viscoelastic response involves a single relaxation process with characteristic time τ_1:

$$G_1 = \frac{\eta_1}{\tau_1}f_1(\omega)(\omega\tau_1+\mathrm{i}), \quad f_1(\omega) = \frac{\omega\tau_1}{1+\omega^2\tau_1^2}. \tag{12}$$

For the filler a purely elastic modulus can be safely assumed, so

$$G_2 = G_2' \quad (\text{real}). \tag{13}$$

Substitution of Eqs. (12) and (13) in Eqs. (9) and (10) gives, for the effective storage modulus,

$$G_{\mathrm{e}}' \cong \frac{\eta_1}{\tau_1}\frac{f_1(\omega)\omega\tau_1}{1-\frac{5}{2}\phi_2} \quad (\varphi_2 < 2/5),$$

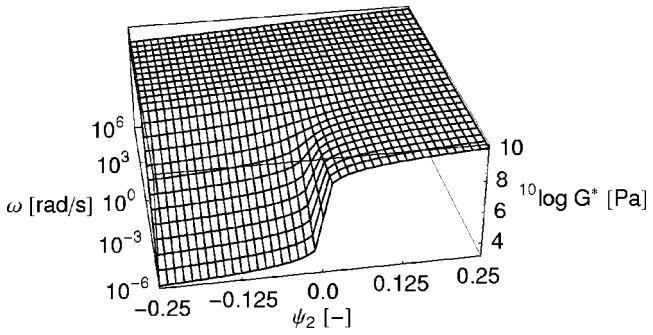

FIG. 7. Results of effective-medium calculations: the effective modulus G_e^* as a function of ω and $\psi_2=\frac{5}{2}\varphi_2-1$. The percolation threshold at $\psi_2=0$ (or $\varphi_2=2/5$) can be clearly distinguished at low frequencies.

$$G_e' \cong \tfrac{2}{3}G_2\left(\tfrac{5}{2}\phi_2-1\right)+\frac{\eta_1}{\tau_1}\frac{f_1(\omega)\omega\tau_1}{\frac{5}{2}\phi_2-1} \quad (\varphi_2>2/5), \quad (14)$$

and for the effective loss modulus,

$$G_e'' \cong \frac{\eta_1}{\tau_1}\frac{f_1(\omega)}{\left|1-\frac{5}{2}\phi_2\right|} \quad (\varphi_2<2/5 \text{ and } \varphi_2>2/5). \quad (15)$$

Finally this allows expressions to be derived for the effective phase angle δ_e as a function of the frequency and filler content:

$$\tan\delta_e \equiv \frac{G_e''}{G_e'} \cong \frac{1}{\omega\tau_1} \quad (\varphi_2<2/5),$$

$$\tan\delta_e \cong \frac{1}{\omega\tau_1+\frac{2}{3}\frac{G_2\tau_1}{\eta_1}\frac{\left(\frac{5}{2}\phi_2-1\right)^2}{f_1(\omega)}} \quad (\varphi_2>2/5). \quad (16)$$

Figure 7 shows the resulting modulus for a composite. G_e^* is plotted as a function of ω and $\psi_2=\frac{5}{2}\varphi_2-1$ around the percolation threshold, $-0.25<\psi_2<0.25$ or $0.30<\varphi_2<0.50$. Equation (8) and (7) is used with substitution of Eqs. (8), (12), and (13). From the experimental data the following values are estimated: $\eta_1=1\times10^9$ Pa s and $\tau_1=1$ s (estimated using Fig. 1 and the fact that $\omega\tau_1=1$ at $\delta=45°$). For G_2 the value of 35 GPa, the shear modulus of $CaCO_3$, was used.

It can be seen that below the percolation threshold the calculated G_e^* increases monotonically with ω, in accordance with the experimental behavior of G_e^*. Above the percolation threshold a plateau develops at low frequencies, again in agreement with the experimental results. At higher frequencies G_1' dominates, and therefore the behavior at high frequencies is quite similar for ψ_2 below and above the percolation threshold [see Eq. (15)]. This was also experimentally observed.

The behavior of δ_e is more complex. From Eq. (16) it is clear that above the percolation threshold the filler will introduce, in addition to the binder time scale τ_1, a second time scale to the system: η_1/G_2; as a result of this, a second peak in δ_e can occur. The separation of the peaks depends on the material parameters of both binder and filler: η_1 and τ_1, and G_2 respectively. Figures 8(a)–8(c) show δ_e as a function of ω and ψ_2. In all cases $\tau_1=1$ s and $G_2=35$ GPa are taken, whereas the second time scale is varied: in Figs. 8(a)–8(c) the ratio τ_1G_2/η_1 equals 10^2 s, 1 s, and 10^{-2} s, respectively. It can be seen that for $\eta_1/G_2<\tau_1$ no peak arises; for $\eta_1/G_2=\tau_1$ there is a critical onset of a peak and for $\eta_1/G_2>\tau_1$ a peak is clearly distinguishable. The latter resembles the experimental behavior of the composites.

A large difference with the experimental behavior is seen for very small ω. When $\psi_2<0$ ($\varphi_2<2/5$) the phase angle δ_e in the calculations ultimately reaches the experimental value of 90°. This means that both in theory and practice the material will flow at very long time scales. However, above the percolation transition, when $\psi_2>0$ ($\varphi_2>2/5$), the calculated δ_e quickly drops to zero, indicating a purely elastic material, which in practice is not observed. This difference can be explained by the fact that EMT assumes that the percolating structure is a continuous second phase of overlapping rigid particles; this structure will then completely dominate the behavior of the composite. In reality such a network cannot arise since there will only be percolation via (nearly) contacting rigid particles, leaving still room for viscous dissipation. The most important conclusion to be drawn from the calculations is that adding a filler to the viscoelastic binder will introduce an additional time scale η_1/G_2 that leads to the appearance of a maximum in $\delta_e(\omega)$; this effect has indeed been observed in the composites. In the experiment, it was also seen that time-temperature superposition fails in the region where δ_e has its maximum. It can now be hypothesized that this failure of TTS originates from the introduction of

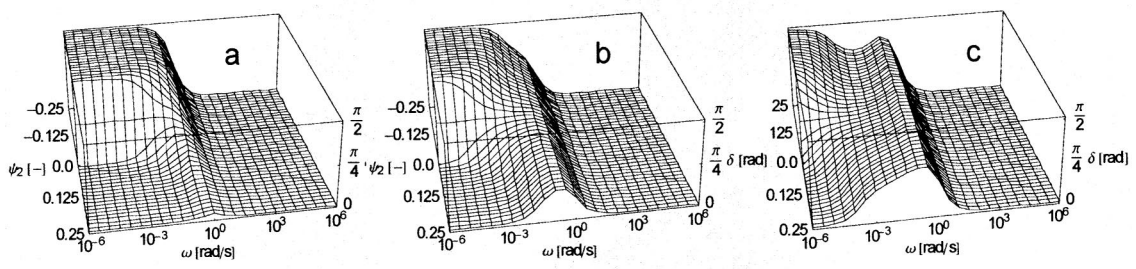

FIG. 8. The effective phase angle δ_e as a function of ω and $\psi_2=\frac{5}{2}\varphi_2-1$, as predicted from effective-medium calculations. In all cases the matrix relaxation time τ_1 equals 1 s; the second time scale, derived from the loss modulus of the matrix and the storage modulus of the filler particles, given by η_1/G_2, is varied: (a) $\eta_1/G_2=10^{-2}$ s, (b) $\eta_1/G_2=10^0$ s, and (c) $\eta_1/G_2=10^2$ s.

the additional time scale η_1/G_2 reflecting the mechanical interplay of the solid particles and the maltene phase.

V. CONCLUSIONS

We have determined the viscoelastic properties of composites consisting of rigid fillers in a microstructured viscoelastic matrix. Rigidity percolation has been observed in these composite materials, shown by a scaling exponent $\alpha = 3.9 \pm 0.6$ for G' near and above a percolation threshold, which is consistent with the value $\alpha \approx 3.75$ from theory and numerical experiments. The elastic network formed is hypothesized to consist of two phases, the mineral-filler particles and (fractal) asphaltene aggregates. This hypothesis is supported by two facts. First, experiments with composites with bidisperse filler assemblies conclusively show that for a given binder the geometry and characteristic length scales of the continuous-matrix space rather than the volume fraction of filler determine whether or not rigidity percolation occurs. Second, effective-medium calculations suggest that the breakdown of time-temperature superposition near the percolation threshold is related to the appearance of a new time scale in the viscoelastic behavior of the composite, as a result of the mechanical interplay between binder and filler.

ACKNOWLEDGMENTS

This work was financed by the Dutch EET research program under Grant No. EETK99029. We thank Shell Global Solutions for providing the residual binder, Rob Hovenkamp (Shell Amsterdam) for advice on binder rheology and sample handling, and Dr. Gerrit Peters (TU Eindhoven) for fruitful discussions.

APPENDIX A: RANDOM PACKINGS OF INTERPENETRABLE SPHERES

In the discussion of the percolation threshold in the monodisperse composites reference has been made to a result from literature [14,19] regarding the effective volume fraction of random packings of monodisperse interpenetrable spheres. Equation (A1) gives an approximation of the effective volume fraction of interpenetrable spheres:

$$\phi_p(\eta,\lambda) = (1 - \eta\lambda^3)\exp\left[-\frac{(1-\lambda^3)}{(1-\eta\lambda^3)^3}\right]A(\eta,\lambda), \quad \text{(A1)}$$

where

$$A(\eta,\lambda) = \exp\left[-\frac{\eta^2\lambda^3(\lambda-1)}{2(1-\eta\lambda^3)^3}[(7\lambda^2+7\lambda-2) - 2\eta\lambda^3 \times(7\lambda^2-5\lambda+1) + \eta^2\lambda^6(5\lambda^2-7\lambda+2)]\right]. \quad \text{(A2)}$$

APPENDIX B: RANDOM BI DISPERSE SPHERE PACKINGS

It is assumed here that the mineral-filler phase is a random packing of polydisperse spheres and that the continuous "pore" space between the mineral particles is filled with maltene phase and fractal asphaltene aggregates. As a characteristic length we use the mean surface-to-surface distance $\lambda_P(R_t)$ that is defined in [14,22].

The probability $h_P(r)dr$ is defined as the probability that the nearest filler particle surface lies at a distance between r and $r+dr$ from the center of a "test particle" with radius R_t. In the present case we identify the asphaltene aggregates with these test particles. Associated with $h_P(r)dr$ is the "exclusion probability" $e_P(r)$,

$$e_P(r) = 1 - \int_{-\infty}^{r} h_P(r')dr', \quad \text{(B1)}$$

the probability that a spherical volume with radius r centered at an arbitrary point does *not* contain other surfaces. Using this definition the mean surface-to-surface distance $\lambda_P(R_t)$ can be defined as

$$\lambda_P(R_t) = \int_{R_t}^{\infty} e_P(r)dr. \quad \text{(B2)}$$

Relations given in [14], for numerical integration of Eq. (B2) to yield $\lambda_P(R_t)$, are repeated below. $e_P(R_t)$ [defined in Eq. (B1)] is related to the quantity $e_V(r)$ with the following definition:

$$e_V(r) = 1 - \int_{-\infty}^{r} h_V(r')dr', \quad \text{(B3)}$$

where $h_V(r)$ is the probability that the nearest particle surface lies at a distance between r and $r+dr$ from an arbitrary point in the system. So $e_V(r)$ is the probability of finding a sphere with a radius r around an arbitrary point that is empty of surfaces. It follows that

$$e_P(R_t) = \frac{e_V(r)}{e_V(R_t)}, \quad r \geqslant R_t. \quad \text{(B4)}$$

In the case of a statistically isotropic 3D system of polydisperse spheres in equilibrium, $e_V(r)$ can be approximated by

$$e_V(r) = \phi_1 \exp[-2\eta S(a_0x^3 + a_1x^2 + a_2x)], \quad \text{(B5)}$$

where

$$S = \frac{\langle R^2\rangle}{\langle R^3\rangle}\langle R\rangle, \quad \text{(B6)}$$

and a_0, a_1, and a_2 are given by

$$a_0 = \frac{4(\langle R\rangle^2/\langle R^2\rangle)(1-\eta)(1-\eta+3\eta S) + 8\eta^2S^2}{(1-\eta)^3}, \quad \text{(B7)}$$

$$a_1 = \frac{6(\langle R\rangle^2/\langle R^2\rangle)(1-\eta)9\eta S}{(1-\eta)^2}, \quad \text{(B8)}$$

$$a_2 = \frac{3}{(1-\eta)}. \quad \text{(B9)}$$

[1] *Asphaltenes and Asphalts*, edited by T. F. Yen and G. V. Chilingarian (Elsevier, Amsterdam, 1994), Vol. 1.
[2] D. Lesueur *et al.*, J. Rheol. **40**, 813 (1996).
[3] J. Ph. Pfeiffer, *The Properties of Asphaltic Bitumen*, Elsevier Polymer Series (Elsevier, Amsterdam, 1950).
[4] H. C. A. Brandt, E. M. Hendriks, M. A. J. Michels, and F. Visser, J. Phys. Chem. **99**, 10430 (1995).
[5] A. J. Markvoort, Master's thesis, TU Eindhoven, 1996.
[6] A. J. Markvoort, H. C. A. Brandt, R. Haswell, and M. A. J. Michels (unpublished).
[7] Shell Internationale Research Maatschappij B.V., M. Reijnhout, Patent No. WO 00/46164, August 10, 2000; M. W. L. Wilbrink, Master's thesis, TU Eindhoven, 2002.
[8] V. Trappe and D. A. Weitz, Phys. Rev. Lett. **85**, 449 (2000).
[9] M. C. Grant and W. B. Russel, Phys. Rev. E **47**, 2606 (1993).
[10] Rheometrics Ares 3LS-4A, Rheometrics Inc.
[11] G. Strobl, *The Physics of Polymers*, 2nd ed. (Springer, Berlin, 1997).
[12] See, e.g., M. O. Marasteanu and D. A. Anderson, Transp. Res. Rec. **1766**, 32 (2001).
[13] C. van der Poel, J. Appl. Chem. **4**, 221 (1954).
[14] S. Torquato, *Random Heterogeneous Materials* (Springer, New York, 2002).
[15] S. Roux, J. Phys. A **19**, L351 (1986).
[16] M. Sahimi, J. Phys. C **19**, L79 (1986).
[17] A. Hansen and S. Roux, Phys. Rev. B **40**, 749 (1989).
[18] C. Moukarzel and P. M. Duxbury, Phys. Rev. E **59**, 2614 (1999).
[19] In [14] this graph is shown, but the source of the points quoted is in error. S. Torquato (personal communication) remarks that two of the points are from [25], two from [26], and two from unpublished work by S. Torquato. The following values are shown in the graph: {0, 0.29}, {0.2, 0.29}, {0.6, 0.31}, {0.67, 0.32}, {0.8, 0.33}, {0.91, 0.41}, {1, 0.64}.
[20] S. B. Lee and S. Torquato, J. Chem. Phys. **89**, 3258 (1988).
[21] D. He, N. N. Ekere, and L. Cai, Phys. Rev. E **65**, 061304 (2002).
[22] B. Lu and S. Torquato, Phys. Rev. A **45**, 5530 (1992).
[23] D. Bruggeman, Ann. Phys. **24**, 636 (1935).
[24] R. Landauer, in *Electrical Transport and Optical Properties of Inhomogeneous Media*, edited by J. C. Garland and D. B. Tanner (AIP, New York, 1978).
[25] E. M. Sevick, P. A. Monson, and J. M. Ottino, J. Chem. Phys. **88**, 1198 (1988).
[26] M. D. Rintoul and S. Torquato, Phys. Rev. Lett. **77**, 4198 (1996).